Localized surface plasmon resonance of single silver nanoparticles studied by dark-field optical microscopy and spectroscopy

Wei Cao,[1] Tao Huang,[2] Xiao-Hong Nancy Xu,[2] and Hani E. Elsayed-Ali[1,3,a)]
[1]*Applied Research Center, Old Dominion University, Newport News, Virginia 23606, USA*
[2]*Department of Chemistry and Biochemistry, Old Dominion University, Norfolk, Virginia 23529, USA*
[3]*Department of Electrical and Computer Engineering, Old Dominion University, Norfolk, Virginia 23529, USA*

(Received 12 August 2010; accepted 7 December 2010; published online 7 February 2011)

Localized surface plasmon resonance (LSPR) of Ag nanoparticles (NPs) with different shapes and disk-shaped Ag NP pairs with varying interparticle distance is studied using dark-field optical microscopy and spectroscopy (DFOMS). Disk-, square-, and triangular-shaped Ag NPs were fabricated on indium tin oxide-coated glass substrates by electron beam lithography. The LSPR spectra collected from single Ag NPs within 5×5 arrays using DFOMS exhibited pronounced redshifts as the NP shape changed from disk to square and to triangular. The shape-dependent experimental LSPR spectra are in good agreement with simulations using the discrete dipole approximation model, although there are small deviations in the peak wavelengths for square- and triangular-shaped NPs. The LSPR spectra of disk-shaped Ag NP pairs with varying interparticle distances were acquired from five different locations across the pair axis. It was clearly observed that the LSPR wavelength redshifts as the interparticle distance decreases, indicating a strong interaction when two Ag NPs are close to each other. © *2011 American Institute of Physics*.
[doi:10.1063/1.3544349]

I. INTRODUCTION

Silver nanoparticles (NPs) have been extensively studied owing to their unique optical properties, i.e., localized surface plasmon resonance (LSPR), that can be utilized to develop nanoscale optical, chemical, and biological sensors.[1–3] LSPR of NPs is generated by coherent oscillations of their surface free electrons when NPs are irradiated by electromagnetic waves in the optical frequency. The observed LSPR spectra depend on NPs' size, shape, and dielectric environments, as well as interparticle interactions. Although there have been numerous reports on the fabrication and LSPR properties of Ag NPs, very few studies have focused on the LSPR of individual NPs, which is critical for developing single-NP sensors. Recently, Song *et al.* used dark-field optical microscopy and spectroscopy (DFOMS) to study the LSPR of individual NPs fabricated by nanosphere lithography (NSL), and showed the ability to observe location-dependent LSPR on individual NPs and correlate that with its three-dimensional (3D) morphology.[4] DFOMS has also been utilized to image and characterize individual Ag NPs in single living cells, in zebrafish embryos, and for single-molecule detection.[5–8]

Previous studies have shown that Ag NPs with controlled size and shape can be prepared in colloidal form using wet chemical methods.[9,10] However, the development of sensing devices often requires NPs to be fabricated on certain types of substrates and integrated with other detection devices. Fabrication techniques used to prepare Ag NPs and NP arrays on flat substrates are mainly based on NSL and electron beam lithography (EBL).[11–14] NSL utilizes hexagonally close-packed nanosphere lattice that self-assembles on a flat substrate as a deposition mask.[11] NSL is a simple, low-cost technique. However, it generally yields only triangular-shaped NPs and hexagonal arrays. Although it is possible to obtain a few other shapes with multiple NSL steps, this process is difficult to control and results in many defects and poor control on NP shape and size. In contrast, EBL not only can be used to fabricate individual NPs as well as NP arrays but also possesses advantages, such as high resolution, precise control on NP shape and size, and versatility of NP array design. Previous reports have demonstrated the fabrication of noble metal (Ag, Au, Pt) NPs and nanowires by EBL.[13,15–17]

The optical properties, especially LSPR, of EBL-derived Ag NPs have been widely characterized using optical microscopy and spectroscopy at micrometer and submicrometer resolution. Corrigan *et al.*[13] studied the fluorescence enhancement on periodic Ag NP arrays and reported greater relative enhancement for triangular-shaped NPs compared to square-shaped ones. Sung *et al.*[18] fabricated two-dimensional (2D) arrays of L-shaped Ag NPs using EBL to study both linear and nonlinear optical properties of NPs without in-plane center of inversion symmetry. They observed two independent LSPR extinction wavelengths with orthogonal polarization for both individual NPs and 2D arrays. The resonant wavelength also shifted as a result of varying interparticle spacing, number of NPs inside an array, as well as dielectric environment by adding solvent. The dipole coupling in 2D NP arrays was also studied by Haynes *et al.*[19] They fabricated both Ag and Au NP arrays consisting of cylindrical and triangular NPs in square and hexagonal arrangements with various interparticle distances. A blueshift in LSPR spectra was observed for both types of NP arrays as

a)Electronic mail: helsayed@odu.edu.

the interparticle distance was decreased. Clearly, when characterized at micrometer scale, the observed LSPR shift is often a result of combined contributions from NP size, shape, and dipole coupling within the NP arrays. Correlating the morphology of a single NP with its characteristic LSPR spectrum is important because this can allow the development of a wide variety of single-NP optical devices for ultrasensitive analysis, e.g., single-molecule detection. Notably, since the morphologies of individual NPs fabricated by EBL can rarely be identical, it becomes essential to characterize and correlate the morphology of the same single NP with its optical properties in order to address fundamental and practical questions related to single NP detectors and NP plasmonic optics.

In this study, we used DFOMS to obtain the LSPR spectra from single Ag NPs and location-dependent LSPR spectra from Ag NP pairs with different interparticle distances. Using specially designed markers fabricated during the EBL process, single NP and group of NP pairs were identified within the NP arrays. Surface and optical characterization were simultaneously performed on the same NP. The ability to identify single NP eliminates the effects of varying NP size and shape on the LSPR spectra. Simulated LSPR spectra for single Ag NP with different shapes using the discrete dipole approximation (DDA) method are compared with the experimental results.

II. EXPERIMENTAL

A. Design and fabrication of Ag NP arrays

The Ag NPs were fabricated using an ELPHY Quantum (Raith, Ronkonkoma, NY) EBL system attached to a scanning electron microscope (SEM, JSM-6060LV, JEOL, Japan). The substrates were microscope glass slides coated with 30 nm thick indium tin oxide (ITO) with resistivity of 70–100 $\Omega\,\mathrm{cm}^{-2}$ (SPI Supplies, West Chester, PA). Each substrate was spin-coated with polymethyl methacrylate (PMMA) positive photoresist (MicroChem, Newton, MA), followed by electron beam exposure at 30 kV. Next, the sample was developed in a methyl isobutyl ketone (MIBK):isopropanol (IPA) developer (MicroChem, Newton, MA) with a ratio of 1:3 for 30 s, then rinsed in IPA for 30 s to stop the development. Ag thin films were then deposited on PMMA-patterned substrates using a thermal evaporation process with deposition rate of ~0.5 Å/s to achieve designed film thickness. Finally, a standard lift-off process was carried out to obtain the NPs with designed size and shape. For the purpose of DFOMS measurements, each NP array was designed to contain 25 (5×5) Ag NPs with interparticle distance of 3.2 μm to minimize the dipole coupling effects. The NP arrays were labeled with specially designed markers so that each NP could be located and identified during surface and optical characterization. NP arrays consisting of 5×5 disk-shaped NP pairs with varying inter-particle distances were also prepared for dipole coupling studies.

B. Surface characterization of Ag NPs

The surface morphology of Ag NPs was characterized using SEM (JSM-6060LV, JEOL, Japan) and atomic force microscopy (AFM, Dimension 3100, Veeco, Santa Barbara, CA).

C. Optical characterization of Ag NPs

The LSPR scattering spectra were acquired using a DFOMS equipped with a high-resolution, multispectral charge-coupled device (CCD) camera (Nuance EX, Cambridge Research & Instrumentation Inc.). The multispectral CCD camera utilizes an optimized, high-throughput, electronically tunable, solid-state filter with spectral range from 450 to 950 nm. The dark-field optical microscope was equipped with a dark-field condenser (Oil 1.43–1.20, Nikon), a microscope illuminator (Halogen lamp, 100 W), and a 100× objective (Nikon Plan fluor 100× oil, iris, SL. N.A. 0.5–1.3, W.D. 0.20 mm), offering the depth of field (focus) of 190 nm. The design and construction of the DFOMS setup was described previously.[4–7] Briefly, the dark-field condenser focuses the light onto the NPs to be characterized. The scattered light enters the objective lens and is then directed to the spectrometer, yielding color images of NPs on a dark background and LSPR spectra of the sample. In this study, the distinctive markers prepared during the EBL process were clearly visible under DFOMS and, thus, allowed us to characterize the same NPs throughout the study.

D. Simulation of LSPR Spectra of Single Ag NPs

We used the DDA method and DDSCAT 7.0, an open source Fortran 90 code developed by Draine and Flatau, to simulate the LSPR spectra of single Ag NPs.[20] In the DDA method, a NP is treated as a cubic array of N polarizable points which represent the polarizability of discrete volumes of material. The polarization of each polarizable point is calculated through an iterative procedure. The LSPR scattering cross-section can be calculated after polarizations of all points are solved in a self-consistent manner. DDA simulations can provide better understanding of the observed LSP spectra of single plasmonic NP. In this study, we adapted the wavelength-dependent dielectric constants of Ag reported by Palik (n=0.209–0.143, for wavelengths of 350–800 nm),[21] and the refractive index of air (n=1.00). We utilized 5 nm as an interdipole separation distance to build a cubic lattice of polarized points (diploes) for each NP and effective radii of 0.0729 μm, 0.0782 μm, and 0.0603 μm for shapes of NPs in Figs. 1(a)–1(c), respectively.

III. RESULTS AND DISCUSSION

Figure 1 shows the SEM images of three 5×5 NP arrays composed of disk-, square-, and triangular-shaped Ag NPs. The diameter of the disk-shaped NPs and the side length of square- and triangular-shaped NPs are ~200 nm. The height of Ag NPs determined by AFM ranged from 30 to 35 nm. Figure 2 shows the AFM images of a square-shaped Ag NP

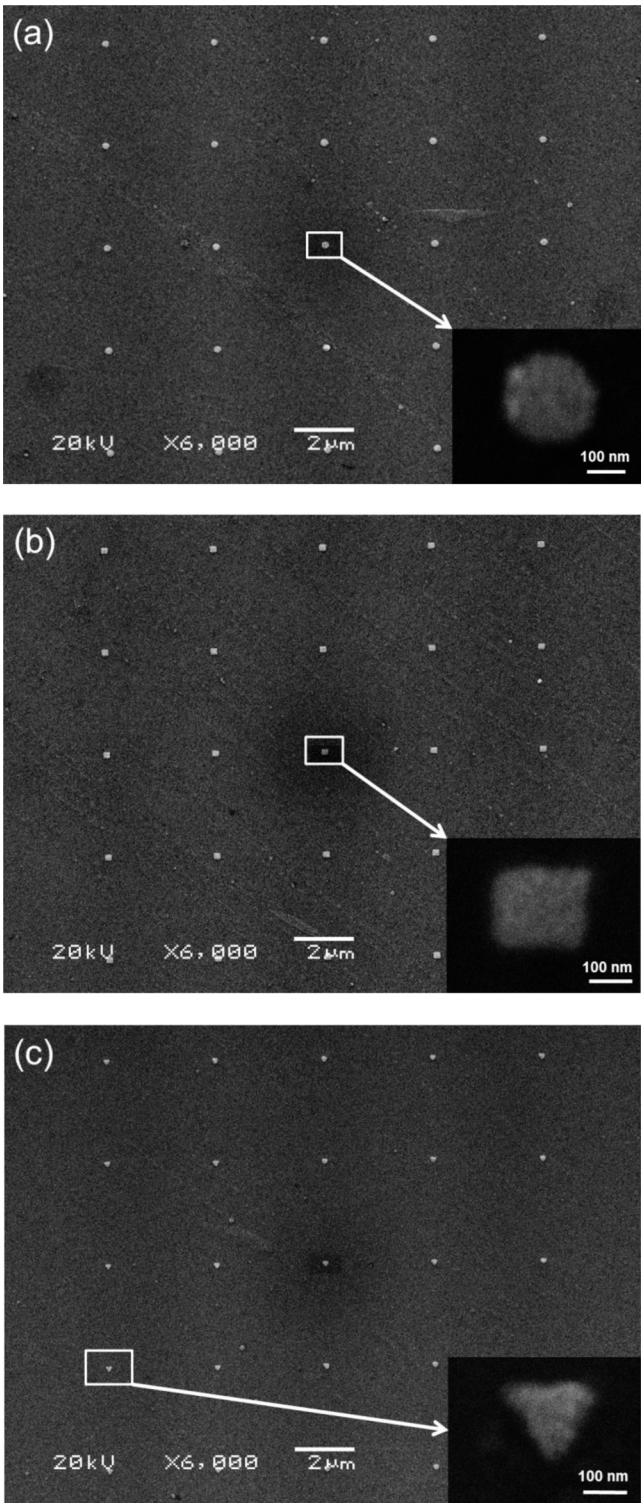

FIG. 1. SEM images of 5×5 Ag NP arrays fabricated by EBL: (a) disks, (b) squares, and (c) triangles. Insets are high magnification images of a single NP.

and the corresponding section analysis illustrating the height measurement. The surface roughness of the NP, measured from Fig. 2(a), is ~10 nm.

The same three NPs with various shapes presented in Fig. 1 were also used for optical characterization, and the results are shown in Fig. 3. The LSPR spectra acquired using DFOMS [Figs. 3(A)(b, i)–3(C)(b, i)] show peak wavelengths (λ_{max}) of 692, 752, and 785 nm for disk-, square-, and

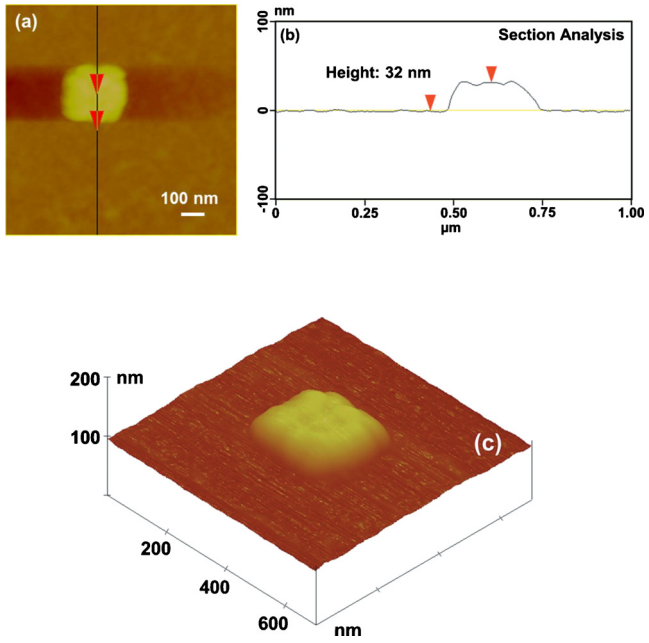

FIG. 2. (Color online) AFM of a square-shaped Ag NP: (a) top view, (b) section analysis showing the NP height of 32 nm, and (c) 3D view.

triangular-shaped NPs, respectively. The redshift in the LSPR spectra, i.e., peak position shifts to a longer wavelength, clearly indicates the effects of the NP shape as the tips become sharper. Such shift was also observed on NSL-prepared Ag NPs by Jenson and co-workers.[22] They measured the LSPR spectra of disk- and triangular-shaped Ag NPs with varying size and showed that the LSPR peak wavelengths of triangular-shaped NPs are longer than those of disk-shaped ones, even for those with smaller size. The LSPR peak shift due to size and interparticle distance variation was also reported by several other research groups.[19,23,24] However, it should be noted that the reported magnitude of shifts varies among published results, which could be due to a combined effect of different factors contributing to the LSPR peak shift since the majority of published LSPR spectra were acquired from an ensemble of NPs. In contrast, the LSPR spectra presented in Fig. 3 were collected from single NPs and, thus, reflected the effects only from NP shapes.

To further understand the experimental results, DDA method was utilized to simulate the LSPR spectra of single Ag NPs with different shapes, and the results are shown in Figs. 3(A)(b, ii)–3(C)(b, ii). It can be seen that, for disk-shaped NPs, the peak wavelength of simulated LSPR spectrum ($\lambda_{p,i}$=689 nm) is in excellent agreement with the experimental data ($\lambda_{p,i}$=692 nm). As for the square- and triangular-shaped NPs, the peak wavelengths of the simulated spectra exhibit small deviations from the experimental data, i.e., $\Delta\lambda_p$=32 nm and $\Delta\lambda_p$=19 nm, respectively. Such deviation may be due to a simplified DDA method, which assumes that the NPs are perfect squares and equilateral triangles, while the real NPs exhibited slightly distorted square and triangular shapes with rounded corners, as shown in SEM and AFM images. Indeed, both experimental results and simulations published previously by other research

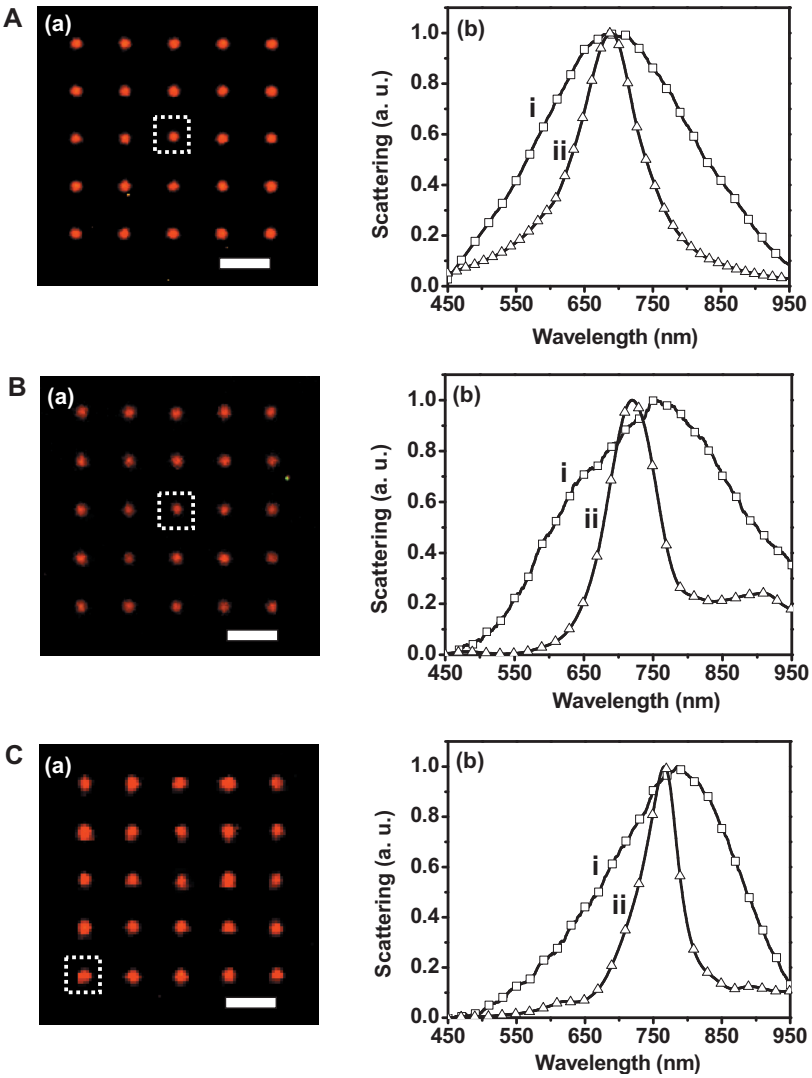

FIG. 3. (Color) Shape-dependent optical properties of single Ag NP using DFOMS and theoretical simulation. (a) Dark-field color images of Ag NP arrays in (A)–(C), which are the same arrays in Figs. 1(a)–1(c), respectively. (b) Normalized LSPR spectra of single Ag NP. These spectra were obtained from NPs shown in the insets of Fig. 1 and indicated by dotted squares in (a). The experimental measurements acquired by DFOMS are labeled as (i) while the DDA simulations are labeled as (ii). All scale bars are 3 μm. Note: single NPs in (a) are imaged under optical diffraction limit and thereby the scale bars in (a) show the distances among NPs, but not the sizes of NPs.

groups demonstrated that shift in LSPR peak wavelength can be a result of rounded or truncated corners of NPs.[25,26] A theoretical study by Ma and co-workers showed that reduced vertex angle for triangular NPs would cause redshift in the calculated LSPR spectra.[27] We also note that the surface morphology of the EBL-fabricated NPs has some surface roughness due to grain boundary formation during the deposition process. This surface feature is different for each NP. Moreover, we have noticed significant changes in morphology in Ag NPs exposed to laboratory air for weeks.[28] In the present study, care was taken to assure that the amount of time the NPs are exposed to laboratory air is far less than that causing NP degradation. Additionally, Chuang *et al.*[29] detected Ag_2O formation at the Ag/PMMA interface while fabricating Ag-coated PMMA periodic arrays using EBL process to study photoactivated fluorescence. The possible effects of a surface oxide layer on the LSPR of Ag NPs and, subsequently, the reliability of final devices may be critical and need to be further investigated.

It should be noted that, in Fig. 3, the full width at half maximum (FWHM) values for the experimental LSPR spectra are higher than those for the simulated data. Generally, the broadening of LSPR spectra for noble metal NPs can be attributed to either electron-surface scattering for small particles or radiation damping for large particles, or both, depending on the particle geometries and dielectric environments.[30] The broadening from radiation damping is also roughly proportional to the volume of the NP. Since the Ag NPs we fabricated in this study are fairly large, radiation damping may significantly contribute to the broadening of experimental LSPR spectra. Moreover, the NPs were fabricated from Ag thin films deposited by a thermal evaporation technique on ITO that generally yields polycrystalline films with relatively high surface roughness, as shown in Fig. 2. Therefore, each NP may be considered as a group of smaller NPs during the optical characterization, thus giving rise to the observed broadening of LSPR spectra due to combined effects of multiple dipole resonances generated from multiple grains within each NP.

Using DFOMS, location-dependent LSPR spectra for Ag NP pairs with varying interparticle distance were also acquired to further study the radiative dipole coupling effects. Figures 4(A)(b)–4(E)(b) show AFM images of five disk-shaped NP pairs with inter-particle distance (D) of about 40 nm, 140 nm, 270 nm, 360 nm, and 460 nm, respectively. The LSPR spectra were collected from five different locations across the NP pair axis marked as i, ii, iii, ii′, and i′ in the optical images in Figs. 4(A)(a)–4(E)(a). The locations were

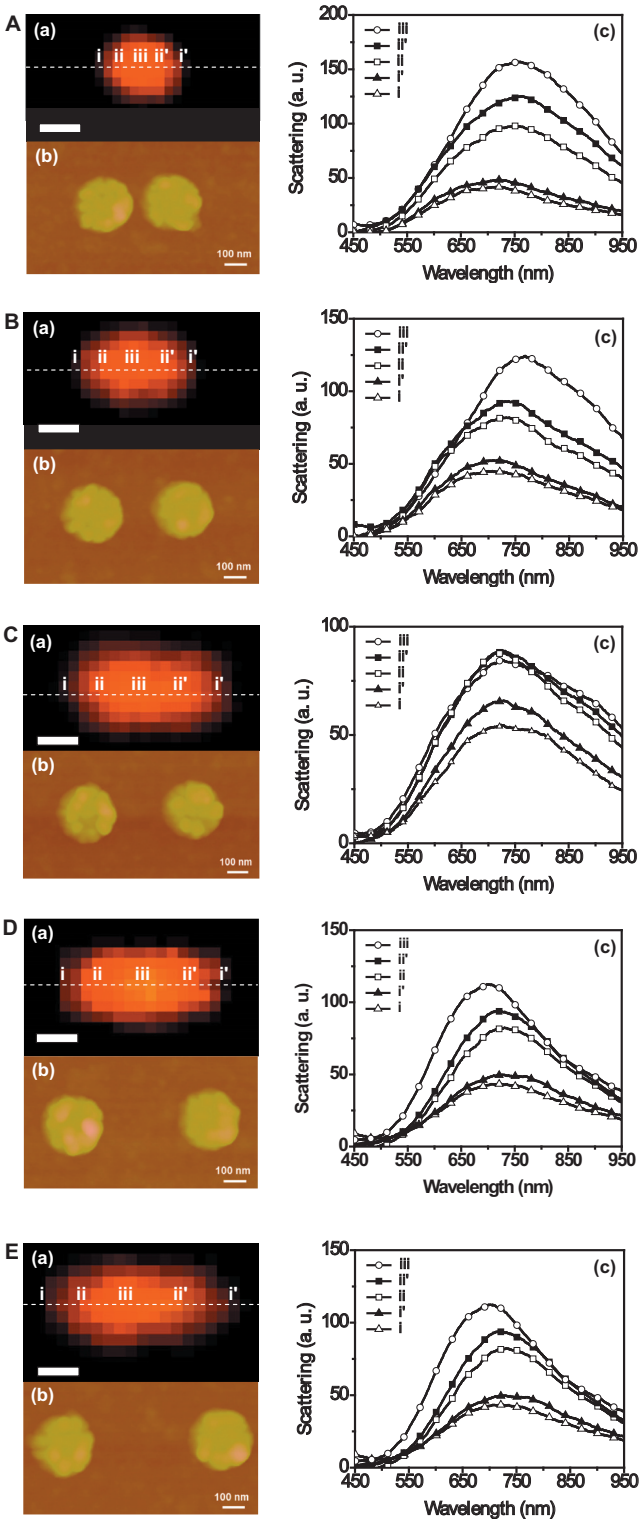

FIG. 4. (Color) Optical and surface characterization of disk-shaped Ag NP pairs using DFOMS and AFM. The dark-field color images in (a) show that the distances between two Ag NPs in each pair are under optical diffraction limit. AFM images in (b) show that the gaps between two Ag NPs are: (A) 40 nm, (B) 140 nm, (C) 270 nm, (D) 360 nm, and (E) 460 nm, respectively. The LSPR spectra of single Ag NPs in (c) acquired at different locations, as marked by the dashed line at (i–iii, ii′–i′) in (a), show that the peak wavelength of LSPR spectra of single Ag NPs depends upon the location and gap between the pair of Ag NPs. All scale bars in (a) are 500 nm.

selected such that pixels i and i′ are close to the end of each NP pair, pixels ii and ii′ at the center of each NP, and pixel iii at the center of the pair axis. Figures 4(A)(c)–4(E)(c) show the LSPR spectra acquired from aforementioned five locations on each NP pair, and the peak wavelengths are summarized in Table I. Clearly, the LSPR spectra for locations ii, iii, and ii′ exhibit pronounced redshifts as the interparticle distance decreases, indicating a strong interaction when two NPs are close to each other. Note that the peak wavelengths of LSPR spectra collected from locations i and i′ show almost no shift, which also illustrates that the LSPR spectrum of a single NP depends on its location within and the surrounding NPs. Similar results were also reported by other research groups that studied the LSPR for Au or Ag NP pairs, although their spectra were acquired from an ensemble of NP pairs that were largely spaced to reduce coupling effects among the pairs.[24,31] Another study involving 2D periodic NP arrays (square and hexagonal) with different lattice spacing conducted by Haynes and co-workers revealed pronounced blueshifts in LSPR spectra with decreasing lattice spacing for both Au and Ag NPs,[19] indicating a more complex coupling effect for ensemble of NPs. They also reported that, unexpectedly, the LSPR spectrum for an isolated NP was not observed even with the largest lattice spacing in their study. In contrast, the LSPR spectra collected in the present study using DFOMS method represent the real optical properties of Ag NP or NP pairs by eliminating the coupling effects from surrounding NPs within an array. Moreover, since the DFOMS system possesses a spatial resolution of single pixel (100 nm), we were able to acquire separate LSPR spectra that resulted solely from either the dipole coupling effects or the NP itself within a NP pair. These spatially resolved spectra provide more accurate information for the development of NP-based sensors.

IV. SUMMARY

Ag NPs with various shapes were fabricated using EBL. The SEM and AFM results showed well-defined disk-, square-, and triangular-shaped NPs with size and height of about 200 nm and 32 nm, respectively. The LSPR spectra were acquired on single Ag NPs within 5×5 arrays using DFOMS and exhibited pronounced redshifts as the tips of a NP became sharper, i.e., NP shape changed from disk to square and to triangular. The shape-dependent experimental LSPR spectra were in good agreement with simulated data using the DDA method despite small deviations on the peak wavelengths for square- and triangular-shaped NPs, which may be attributed to a simplified DDA model used for simulation. The radiative dipole coupling within Ag NP pairs with varying interparticle distance was also studied by collecting the LSPR spectra from different locations on the pair axis. It was clearly observed that the LSPR wavelength redshifts as the interparticle distance decreases, indicating a strong interaction when two Ag NPs are close to each other. The magnitude of the redshift varies for the LSPR spectra acquired at different locations, which also illustrates that the LSPR spectrum of a single NP depends on its location within a NP array and the surrounding NPs. This study provides effective means to investigate the optical properties of isolated Ag

TABLE I. Summary of location-dependent LSPR spectra of disk-shaped Ag NP pairs.

NP pair	Interparticle distance (D) (nm)	λ_p (nm) i	ii	iii	ii′	i′
A	40	720	760	765	763	720
B	140	717	738	766	738	717
C	270	727	727	725	725	727
D	360	725	727	714	727	725
E	460	725	727	714	727	725

NPs and offers experimental data that may benefit the development of high sensitivity chemical and biological sensing devices.

ACKNOWLEDGMENTS

This work is supported in part by the National Science Foundation NIRT (Grant Nos. BES-0507036, DMR 0420304, and MRI-0821180) and NIH (Grant No. R01 GM076440). W.C. and T.H. contributed equally to this work.

[1]B. Sepúlveda, P. C. Angelome, L. M. Lechuga, and L. M. Liz-Marzan, Nano Today **4**, 244 (2009).
[2]J. N. Anker, W. P. Hall, O. Lyandres, N. C. Shah, J. Zhao, and R. P. Van Duyne, Nature Mater. **7**, 442 (2008).
[3]J. Zhao, X. Y. Zhang, C. R. Yonzon, A. J. Haes, and R. P. Van Duyne, Nanomedicine **1**, 219 (2006).
[4]Y. J. Song, P. D. Nallathamby, T. Huang, H. E. Elsayed-Ali, and X. H. N. Xu, J. Phys. Chem. C **114**, 74 (2010).
[5]S. V. Kyriacou, W. J. Brownlow, and X. H. N. Xu, Biochemistry **43**, 140 (2004).
[6]T. Huang, P. D. Nallathamby, D. Gillet, and X. H. N. Xu, Anal. Chem. **79**, 7708 (2007).
[7]T. Huang, P. D. Nallathamby, and X. H. N. Xu, J. Am. Chem. Soc. **130**, 17095 (2008).
[8]K. J. Lee, P. D. Nallathamby, L. M. Browning, C. J. Osgood, and X. H. N. Xu, ACS Nano **1**, 133 (2007).
[9]V. K. Sharma, R. A. Yngard, and Y. Lin, Adv. Colloid Interfac. **145**, 83 (2009).
[10]A. R. Tao, S. Habas, and P. D. Yang, Small **4**, 310 (2008).
[11]J. C. Hulteen and R. P. Vanduyne, J. Vac. Sci. Technol. A **13**, 1553 (1995).
[12]W. Huang and M. A. El-Sayed, Eur. Phys. J. Spec. Top. **153**, 223 (2008).
[13]T. D. Corrigan, S. Guo, R. J. Phaneuf, and H. Szmacinski, J. Fluoresc. **15**, 777 (2005).
[14]L. Gunnarsson, T. Rindzevicius, J. Prikulis, B. Kasemo, M. Kall, S. L. Zou, and G. C. Schatz, J. Phys. Chem. B **109**, 1079 (2005).
[15]E. M. Hicks, S. L. Zou, G. C. Schatz, K. G. Spears, R. P. Van Duyne, L. Gunnarsson, T. Rindzevicius, B. Kasemo, and M. Kall, Nano Lett. **5**, 1065 (2005).
[16]A. M. Contreras, J. Grunes, X. M. Yan, A. Liddle, and G. A. Somorjai, Top. Catal. **39**, 123 (2006).
[17]R. Juhasz, N. Elfstrom, and J. Linnros, Nano Lett. **5**, 275 (2005).
[18]J. Sung, E. M. Hicks, R. P. Van Duyne, and K. G. Spears, J. Phys. Chem. C **111**, 10368 (2007).
[19]C. L. Haynes, A. D. McFarland, L. L. Zhao, R. P. Van Duyne, G. C. Schatz, L. Gunnarsson, J. Prikulis, B. Kasemo, and M. Kall, J. Phys. Chem. B **107**, 7337 (2003).
[20]B. T. Draine and P. J. Flatau, J. Opt. Soc. Am. A **11**, 1491 (1994).
[21]E. D. Palik, *Handbook of Optical Constants of Solids* (Academic, Orlando, 1985).
[22]T. R. Jensen, M. D. Malinsky, C. L. Haynes, and R. P. Van Duyne, J. Phys. Chem. B **104**, 10549 (2000).
[23]B. K. Canfield, S. Kujala, K. Laiho, K. Jefimovs, T. Vallius, J. Turunen, and M. Kauranen, J. Nonlinear Opt. Phys. Mater. **15**, 43 (2006).
[24]P. K. Jain, W. Y. Huang, and M. A. El-Sayed, Nano Lett. **7**, 2080 (2007).
[25]J. J. Mock, M. Barbic, D. R. Smith, D. A. Schultz, and S. Schultz, J. Chem. Phys. **116**, 6755 (2002).
[26]K. L. Kelly, E. Coronado, L. L. Zhao, and G. C. Schatz, J. Phys. Chem. B **107**, 668 (2003).
[27]W. Y. Ma, H. Yang, J. P. Hilton, Q. Lin, J. Y. Liu, L. X. Huang, and J. Yao, Opt. Express **18**, 843 (2010).
[28]W. Cao and H. E. Elsayed-Ali, Mater. Lett. **63**, 2263 (2009).
[29]C. M. Chuang, M. C. Wu, W. F. Su, K. C. Cheng, and Y. F. Chen, Appl. Phys. Lett. **89**, 061912 (2006).
[30]M. Hu, C. Novo, A. Funston, H. N. Wang, H. Staleva, S. L. Zou, P. Mulvaney, Y. N. Xia, and G. V. Hartland, J. Mater. Chem. **18**, 1949 (2008).
[31]C. Tabor, R. Murali, M. Mahmoud, and M. A. El-Sayed, J. Phys. Chem. A **113**, 1946 (2009).